Matter and Radiation at Extremes | RESEARCH ARTICLE | scitation.org/journal/mre

Fabrication of solid CH-CD multilayer microspheres for inertial confinement fusion

Cite as: Matter Radiat. Extremes 6, 025901 (2021); doi: 10.1063/5.0033103
Submitted: 25 October 2020 • Accepted: 5 January 2021 •
Published Online: 2 February 2021

View Online Export Citation CrossMark

Meifang Liu,[1] Xing Ai,[1] Yiyang Liu,[1] Qiang Chen,[1] Shuai Zhang,[1] Zhibing He,[1] Yawen Huang,[2] and Qiang Yin[1,a)]

AFFILIATIONS

[1]Research Center of Laser Fusion, China Academy of Engineering Physics, Mianyang, China
[2]State Key Laboratory of Envronment-Friendly Energy Materials, Southwest University of Science and Technology, Mianyang, China

[a)]**Author to whom correspondence should be addressed:** qyin839@sina.com

ABSTRACT

Deuterated polymer microspheres can be used as a neutron source in conjunction with lasers because thermonuclear fusion neutrons can be produced efficiently by collisions of the resulting energetic deuterium ions. A new type of solid deuterated polymer microsphere with a carbon hydrogen–carbon deuterium (CH-CD) multilayer has been designed for preparing the target for inertial confinement fusion (ICF) experiments. To fabricate these solid CH-CD multilayer microspheres, CH beads are first fabricated by a microfluidic technique, and the CD coating layer is prepared by a plasma polymerization method. Both polystyrene (PS) and poly(α-methylstyrene) (PAMS) are used as the material sources for the CH beads. The effects of the PS and PAMS materials on the quality of the solid CH beads and the resulting CH-CD multilayer polymer microspheres are investigated. The solid PS beads have better sphericity and a smoother surface, but large vacuoles are observed in solid PS-CD multilayer microspheres owing to the presence of residual fluorobenzene in the beads and a glass transition temperature of the solid PS beads that is lower than the temperature of plasma polymerization. Therefore, solid PAMS beads are more suitable as a mandrel for fabricating solid CH-CD multilayer polymer microspheres. Solid CH-CD multilayer microspheres with specified size have been successfully prepared by controlling the droplet size and the CD deposition rate and deposition time. Compared with the design value, the diameter deviation of the inner CH beads and the thickness deviation of the CD layer can be controlled within 20 μm and 2 μm, respectively. Thus, an approach has been developed to fabricate solid CH-CD multilayer microspheres that meet the physical design requirements for ICF.

© 2021 Author(s). All article content, except where otherwise noted, is licensed under a Creative Commons Attribution (CC BY) license (http://creativecommons.org/licenses/by/4.0/). https://doi.org/10.1063/5.0033103

I. INTRODUCTION

A variety of physical experiments, such as central hotspot ignition,[1] fast ignition,[2] shock ignition,[3] and spherically convergent plasma fusion,[4] have been performed to investigate inertial confinement fusion (ICF) in recent years. Different types of microspheres, such as glass shells,[5] polymer microspheres,[6–8] and diamond spheres,[9] have been used for preparing the targets in these experiments. Deuterated polymer microspheres are used as the target capsules in some experiments because thermonuclear fusion neutrons can be produced efficiently by the collisions of the resulting energetic deuterium ions.[10–13] Therefore, investigation of fabrication techniques for such deuterated polymer microspheres is of great importance.

To fabricate deuterated polymer microspheres meeting the physical requirements for ICF experiments, deuterated polystyrene (DPS) has been synthesized by radical polymerization and purified to remove hydrophilic substances.[14–16] DPS shells and beads have been successfully prepared by a microfluidic technique, and their quality has been improved by optimization of density matching, interfacial tension, curing rate, and other factors.[17–20] Millimeter-scale DPS shells have been used as targets in an experimental investigation of a laser-driven spherically convergent plasma fusion scheme, and thermonuclear neutrons have been produced stably and efficiently.[4] DPS-CH double-layer shells have also been used for preparing targets in a fast ignition experiment, and a significant enhancement in neutron yield has been achieved.[21]

A new type of solid deuterated polymer microsphere with a carbon hydrogen–carbon deuterium (CH-CD) multilayer has been designed to investigate the kinetic effects arising in the interpenetration layer between the corona plasma of the compressed bead and the plasma produced by the laser and the inner wall of the hohlraum because the solid CH bead can suppress implosion neutron and hydrodynamic instabilities, while the CD layer can produce a measurable D–D neutron yield.[22] According to the physical design, the allowable deviations are 20 μm and 2 μm for the diameter of the

©Author(s) 2021

inner CH bead and the thickness of the CD layer, respectively. Moreover, the size of the vacuoles in these polymer microspheres must be less than 5 μm. The objective of the present work is to fabricate solid CH-CD multilayer polymer microspheres meeting the physical design requirements. Both polystyrene (PS) and poly(α-methylstyrene) (PAMS) are used as the source of the solid CH bead, while a deuterated glow discharge polymer (GDP) is used for the CD layer. The effect of the PS and PAMS materials on the quality of the CH beads and the resulting CH-CD multilayer polymer microspheres is investigated, and the related mechanisms are discussed.

II. EXPERIMENTAL

A. Materials

PS was purchased from Acros Organics, Inc., and PAMS was obtained from Southwest University of Science Technology, China.[23] The weight-average molecular weights $\bar{M}_w$ of the PS and PAMS materials measured by gel permeation chromatography (GPC) were 222 000 and 441 000, respectively, while their respective molecular weight distributions were 1.9 and 1.1, as shown in Fig. 1 and Table I. Poly(vinyl alcohol) (PVA, with $\bar{M}_w$ = 13 000–23 000 and 87%–89% hydrolysis degree), fluorobenzene (FB), and anhydrous calcium chloride ($CaCl_2$) were purchased from Sigma-Aldrich Co., Shanghai Aladdin Bio-Chem Technology Co., Ltd., and Chengdu Kelong Chemical Reagent Factory, respectively.

B. Preparation of CH-CD multilayer polymer microspheres

The solid CH-CD multilayer polymer microspheres were prepared by a microfluidic technique and plasma polymerization (Fig. 2). The details of the solid CH beads are given in Ref. 17. An 8.0 wt. % polymer/FB solution was used as the oil (O) phase, while an aqueous solution containing 2.0 wt. % PVA and 2.0 wt. % $CaCl_2$ was used as the water (W) phase. The deuterated glow discharge polymer (D-GDP) was then deposited on the polymer beads by a lower-pressure plasma polymerization instrument.[24] Deuterium gas and deuterated methane were used as the carrier and polymer sources, respectively, for preparing the CD layer.

TABLE I. Weight-average molecular weight $\bar{M}_w$, number-average molecular weight $\bar{M}_n$, and molecular weight distribution $\bar{M}_w/\bar{M}_n$ of the PS and PAMS materials.

Sample	$\bar{M}_w$	$\bar{M}_n$	$\bar{M}_w/\bar{M}_n$
PS	222 000	118 000	1.9
PAMS	441 000	410 000	1.1

C. Characterization

The thermal stabilities of the materials and corresponding beads were measured by thermogravimetric analysis (TGA) at 10 °C/min from 50 °C to 600 °C. The flow rate of the nitrogen atmosphere was 40 ml/min. The glass transition temperature was measured by differential scanning calorimetry (DSC) at 10 °C/min from 50 °C to 220 °C. The flow rate of the nitrogen atmosphere was also 40 ml/min. A second scan was also run to eliminate the thermal history after an initial scan that was followed by cooling. The pyrolysis products of the materials and the beads were characterized by pyrolysis–gas chromatography–mass spectrometry (PY-GC-MS) at 500 °C for 30 s. Both the O droplets (which were composed of polymer solution) and the resulting shells were characterized by a digital microscope. The surfaces of the polymer microspheres and their cross-sectional morphologies were characterized by scanning electron microscopy (SEM). The beads were broken in liquid nitrogen, and the fractured surfaces before the SEM characterization were sputter-coated with gold under argon for 1 min. The polymer microspheres were also characterized by a computed tomography technique to observe the locations of vacuoles.

The diameters of the microspheres were measured by a measuring microscope. From the experimental results for the diameter, the out-of-roundness δ_{OOR}, defined as half the difference between the maximum and minimum outer diameters of a torus projected from the microsphere in six directions, was used to characterize the sphericity. The surface roughness was measured by both a white light interferometer and a sphere mapper. From the results of the white light interferometry, the average roughness R_a, root-mean-squared roughness R_q, and maximum height roughness R_t were calculated over the entire measured array as follows:

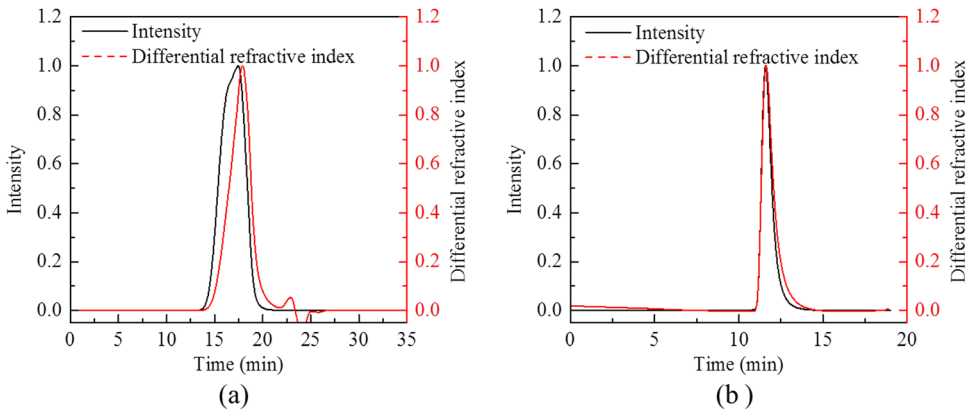

FIG. 1. GPC results for (a) PS and (b) PAMS materials.

©Author(s) 2021

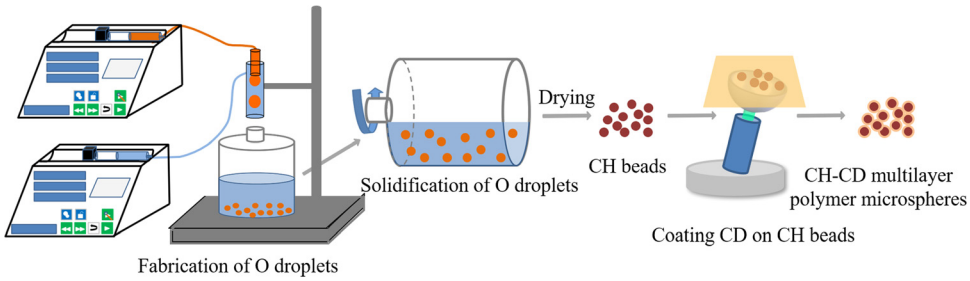

FIG. 2. Schematic illustration of CH-CD multilayer polymer microspheres.

$$R_a = \frac{1}{n}\sum_{i=1}^{n}|Z_i - \bar{Z}|, \tag{1}$$

$$R_q = \sqrt{\frac{1}{n}\sum_{i=1}^{n}(Z_i - \bar{Z})^2}, \tag{2}$$

$$R_t = Z_{\max} - Z_{\min}, \tag{3}$$

where n is the number of points in the entire measured array, and Z_i, $\bar{Z}$, $Z_{\max}$, and $Z_{\min}$ are the measured data, the arithmetic mean, the maximum height, and the minimum height, respectively.

III. RESULTS AND DISCUSSION

A. Fabrication of solid CH beads

To obtain solid CH beads meeting the physical design requirements, an elaborate fabrication scheme was devised. The diameter of the CH beads was required to be 480 μm in this work, and so, according to conservation of mass, the average diameter of the corresponding droplets was calculated to be 1128 μm when the polymer mass fraction of the oil phase was 8.0%.[17] PS beads of 492 μm average diameter and PAMS beads of 484 μm average diameter were successfully prepared by the same microfluidic technique (Fig. 3). The diameter variations of the PS and PAMS beads in each batch were 2 μm and 4 μm, respectively. The coefficients of variation (CV) of the diameter were less than 1.0%, indicating good monodispersity. Therefore, whether PS or PAMS material was used had no significant effect on controlling bead size. Moreover, the diameter deviation from the required value (480 μm) was less than 20 μm, meeting the physical design requirement.

The sphericity, surface roughness, and residual solvent of the solid CH beads were determined to investigate the effect of the PS and PAMS materials on the quality of the beads. For both PS and PAMS beads, all the δ_{OOR} values were less than 1.0 μm, which meant that the sphericity was higher than 99.6%, i.e., all the beads had good sphericity. The PS beads showed better sphericity than the PAMS beads

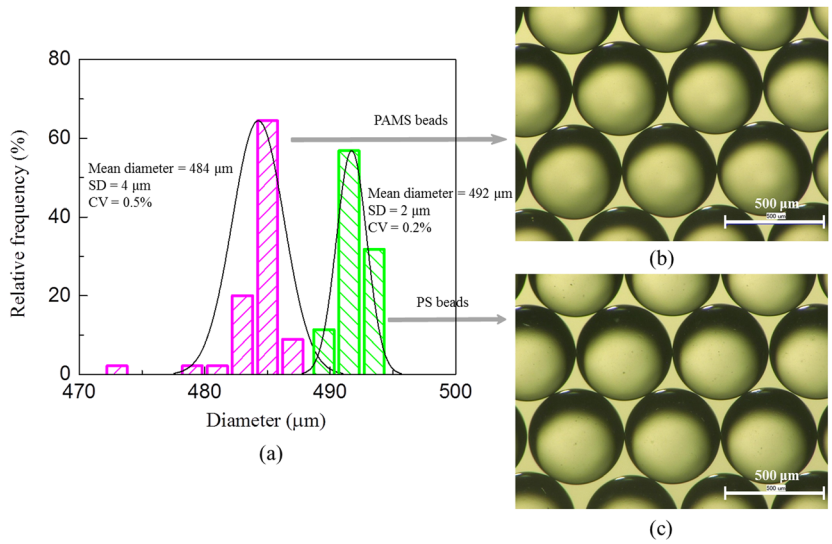

FIG. 3. (a) Diameter distributions of solid PAMS beads (purple bars) and PS beads (green bars). (b) Optical micrograph of PAMS beads of 484 μm diameter. (c) Optical micrograph of PS beads of 492 μm diameter.

©Author(s) 2021

[Figs. 4(a) and 4(b)]. The mode-power curve over modes 2–10 of the PS beads was lower [Fig. 4(b)], and the R_a, R_q, and R_t values of the PS beads were less than those of the PAMS beads [Fig. 4(c)], indicating better surface quality of the PS beads.

The differences in sphericity and surface roughness are probably due to the different molecular weights and molecular structures of PS and PAMS. The viscosity of the PAMS solution is higher than that of the PS solution, and the PAMS chain length is greater, because the weight-average molecular weight of the PAMS is higher. Generally, the initial droplets are not ideal spheres, and they take some time to become spherical. Owing to the higher viscosity, the time to reach a spherical shape is shorter for PAMS droplets, and their ability to regain ideal sphericity is also weaker, which is unfavorable for improving sphericity. The higher viscosity also makes the rearrangement of PAMS chains more difficult. Moreover, there is one more side group (a methyl group) in

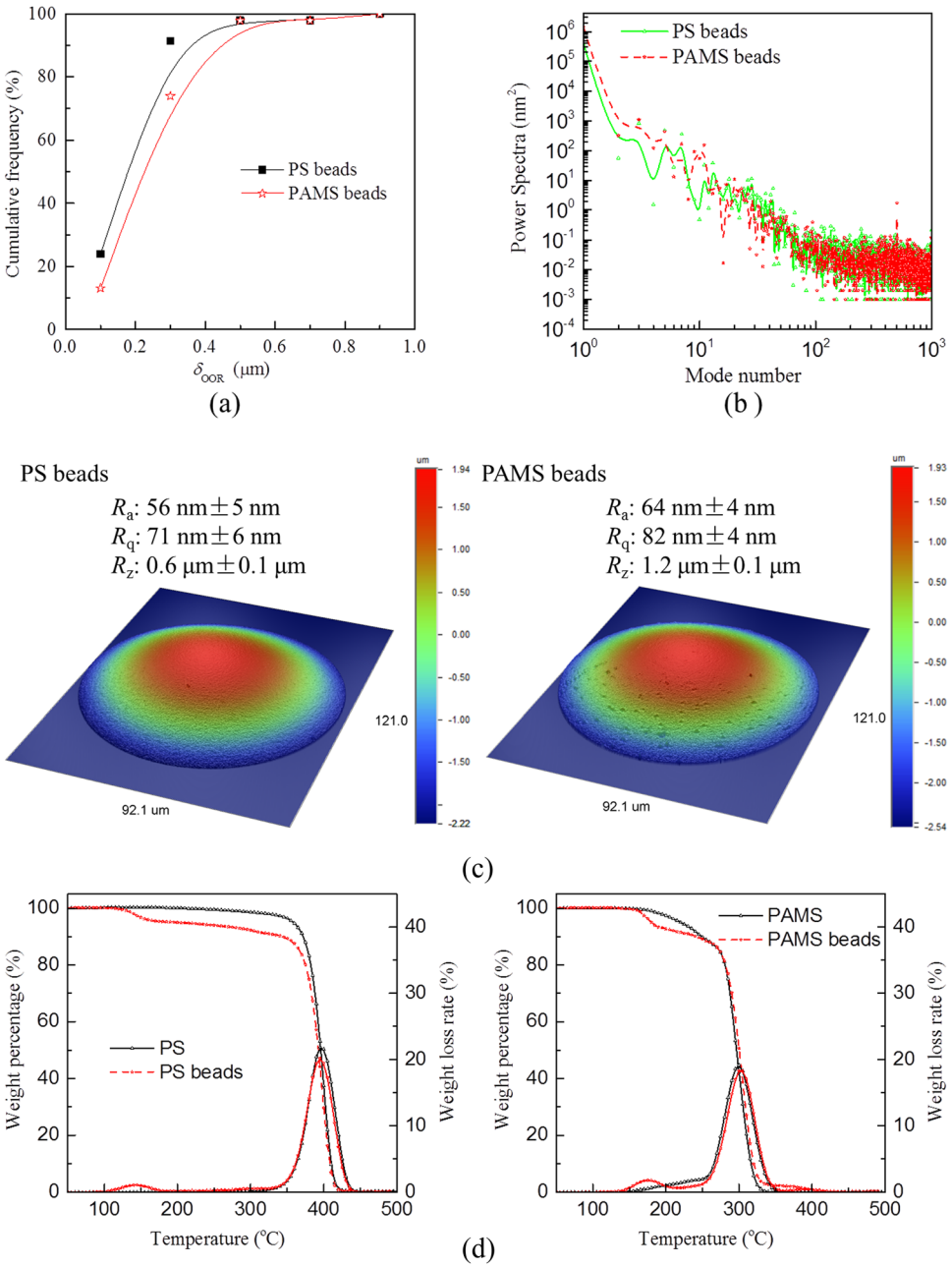

FIG. 4. Effect of PS and PAMS materials on the quality of solid CH beads: (a) sphericity; (b) power spectrum; (c) surface roughness; (d) thermal properties.

©Author(s) 2021

TABLE II. Weight loss percentage of PS material, PS beads, PAMS material, and PAMS beads at 200 °C.

Sample	PS	PS beads	PAMS	PAMS beads
Weight loss percentage at 200 °C (%)	0	5.0	2.5	7.3

the PAMS chain compared with the PS chain, which imposes more restrictions on the torsion about σ bonds in the backbone of the chain, and so the steric exclusion increases and the PAMS backbone becomes less flexible.[25] It has been reported that the surface roughness of polymer films is probably affected by the static structure of the polymer.[26] Therefore, the higher surface roughness of the PAMS beads can probably be attributed to the lower rearrangement capability and lower flexibility of the PAMS chain.

Moreover, our previous work has confirmed that complete removal of the FB remaining in the beads is a challenging task. The amount of residual solvent can be evaluated by TGA.[17] As shown in Fig. 4(d), the TGA curve of the beads is similar to that of the corresponding material, except for earlier weight loss due to evaporation of the residual FB used in the fabrication of the beads. The weight loss of the PS beads was 5.0%, while that of the PS material was zero at 200 °C (Table II), indicating that the mass fraction of the remaining FB was 5.0% in the PS beads. The weight loss of the PAMS material was 2.5% at 200 °C (Table II), which was due to the residual toluene from the synthesis, as confirmed by the PY-GC-MS results (Fig. 5). There are two peaks at about 4.5 min and 6.7 min, respectively, in the GC plot of the PAMS material [Fig. 5(a)]. The corresponding mass spectrum of the product eluting at about 4.5 min [Fig. 5(b)] shows high ion signals at mass-to-charge ratios m/z of 91 and 92, which are typical ion peaks of toluene.[27] The corresponding mass spectrum of the product eluting at about 6.7 min [Fig. 5(c)] shows high ion signals at $m/z = 118$, which are typical ion peaks of α-methylstyrene. Compared with the weight loss of

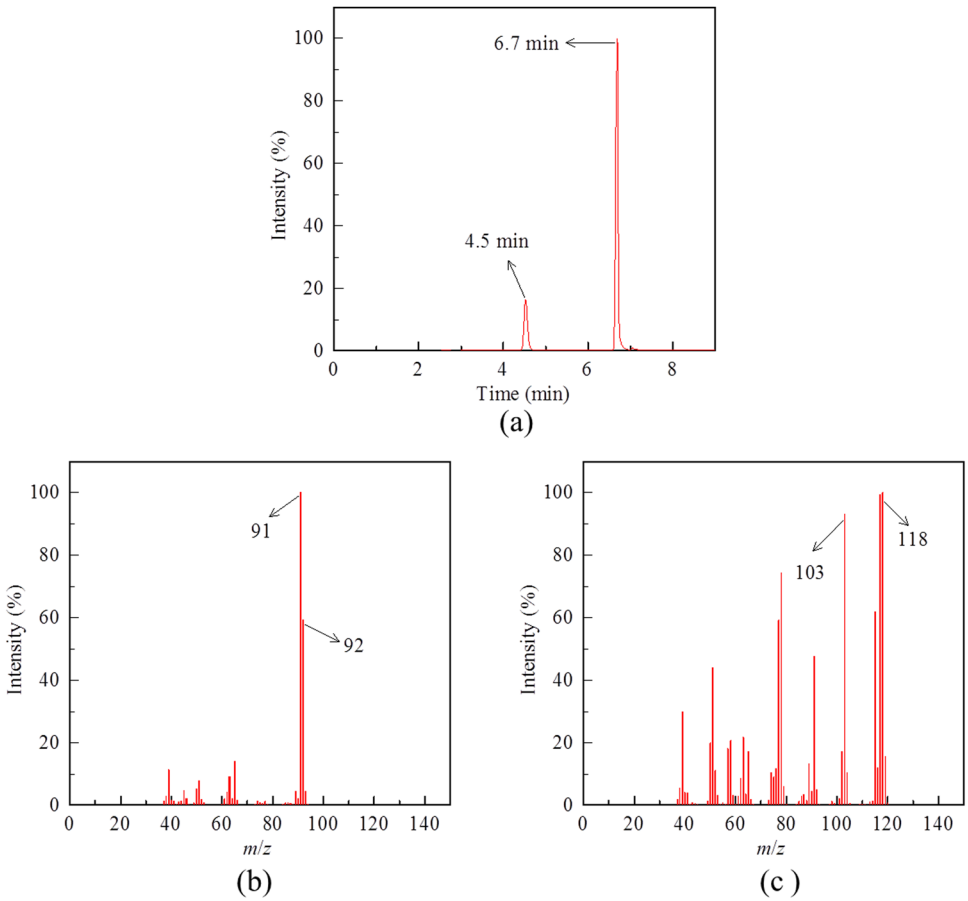

FIG. 5. Pyrolysis products of PAMS material at 500 °C for 30 s: (a) GC plot; (b) mass spectrum for $t = 4.5$ min; (c) mass spectrum for $t = 6.7$ min.

©Author(s) 2021

the PAMS material (2.5%), that of the PAMS beads increased to 7.3% at 200 °C (Table II), implying that the mass fraction of residual FB was 4.8% in the PAMS beads. Therefore, whether PS or PAMS material was used had no significant effect on the amount of residual FB.

B. Fabrication of solid CH-CD multilayer polymer microspheres

To fabricate solid CH-CD multilayer polymer microspheres, a CD layer was deposited on the polymer beads by plasma polymerization with a working pressure of 10 Pa, a power of 15 W, and a D_2/CD_4 gas flow of 2/1. The average diameter of the PAMS-CD multilayer microspheres was 516 μm, and the variation coefficient of the diameter was less than 1.0%. Thus, the average wall thickness of the CD layer was 16.0 μm. The CD deposition rate v can be calculated by

$$v = \frac{d_m - d_b}{t}, \tag{4}$$

where d_m and d_b are the diameters of the multilayer microspheres and the beads, respectively, and t is the deposition time. Here, the deposition

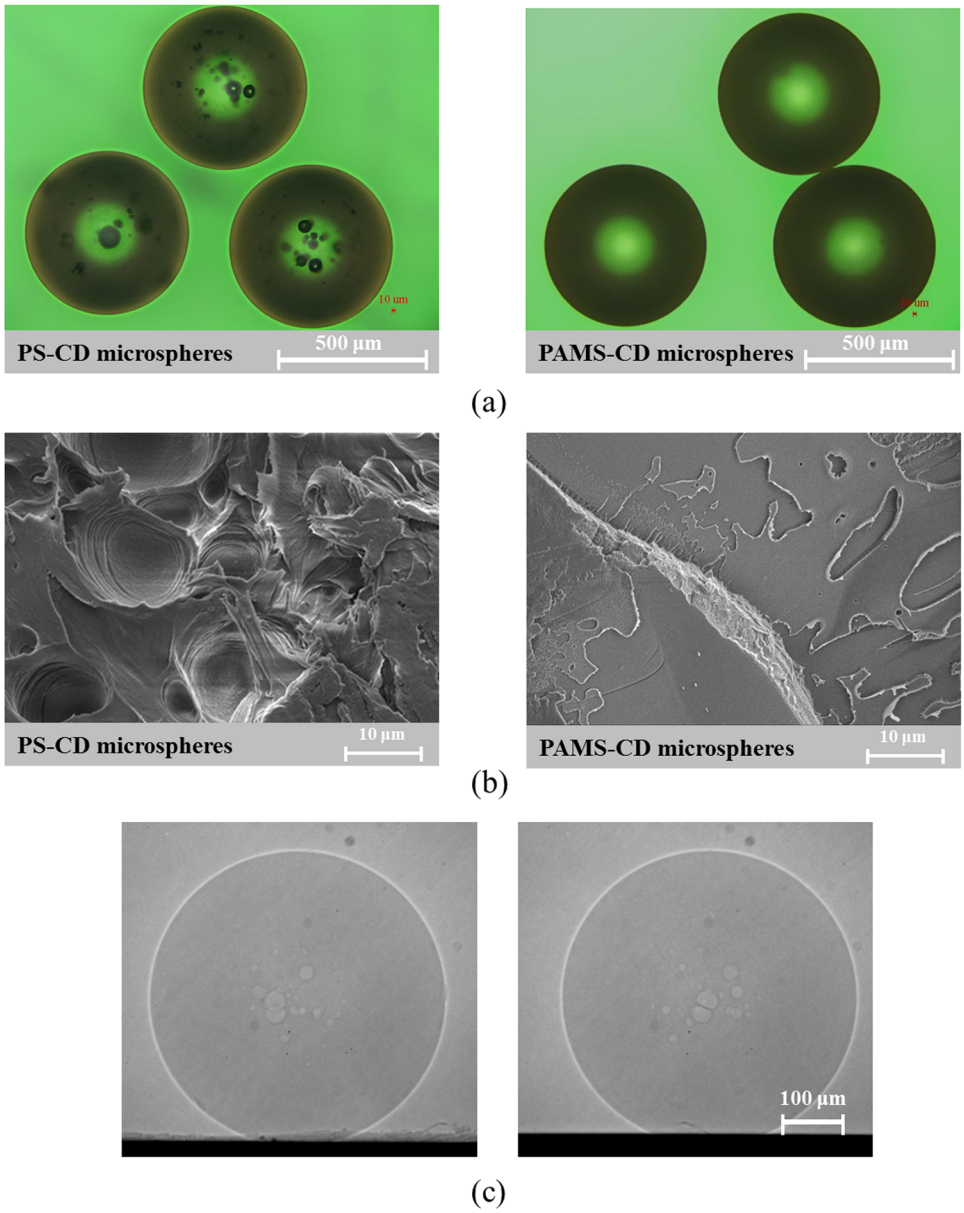

FIG. 6. Micrographs of solid CH-CD multilayer polymer microspheres: (a) optical micrography; (b) cross-sectional SEM images; (c) computed tomography image of PS-CD microspheres from two directions.

©Author(s) 2021

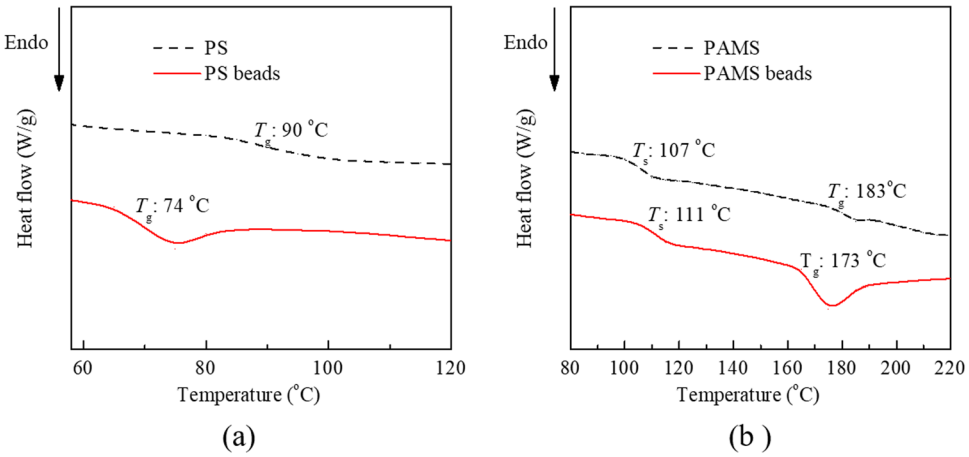

FIG. 7. DSC first–scan curves of the polymer materials and corresponding beads: (a) PS material and beads; (b) PAMS material and beads.

time for the PAMS beads was 65 h. Hence, the calculated CD deposition rate was 0.25 μm/h, which was higher than the CH deposition rate.[28,29] We have confirmed that the reproducibility of the CD deposition rate was good. Therefore, with the calculated CD deposition rate, the wall thickness of the CD layer can be estimated by controlling the deposition time. The deposition time for the PS beads was 48 h, and the average diameter of the PS-CD multilayer microspheres was 519 μm. Thus, the average wall thickness of the CD layer and the calculated CD deposition rate were 13.5 μm and 0.28 μm/h, respectively. The calculated CD deposition rate for PS beads was a little higher than that for PAMS beads, probably owing to many large vacuoles appearing in the PS-CD multilayer microspheres [Fig. 6(a)], which may increase the diameter of the PS-CD beads.

As shown in Fig. 6, many vacuoles were observed by optical microscopy in the PS-CD multilayer microspheres, and the sizes of these large vacuoles were in the range 5 μm–30 μm. Moreover, the large vacuoles were in the central region of the PS-CD multilayer microspheres, far from the surface [Fig. 6(c)]. There were no large vacuoles in the PAMS-CD multilayer microspheres: the vacuoles that can be seen in the cross-sectional SEM image of such a microsphere in Fig. 6(b) are smaller than 2 μm. Hence, the PAMS-CD multilayer microspheres can meet the physical design requirements. This indicates that PAMS beads are more suitable for use as a mandrel for the fabrication of CH-CD multilayer polymer beads. Moreover, it is of interest to determine why the large vacuoles appear only in the PS-CD multilayer microspheres.

Figure 7 shows the first DSC scan for the polymer materials and the corresponding beads. There is only a single dip for the PS material and beads. Two dips appear in the DSC first–scan curves of the PAMS material and beads, although there was only one dip at about 160 °C in the second scan. The first dips in the scans of the PAMS material and beads can probably be attributed to evaporation of toluene remaining in the material and FB remaining in the beads, respectively. Moreover, compared with the glass transitions of the PS and PAMS materials, those of the corresponding beads were broadened, and the glass transition temperatures of the beads shifted to a lower range, accompanied by a broad endothermic peak, also due to the solvent effect of the FB remaining in the beads.[30,31] Specifically, the residual FB in the PS beads led to a decrease in the glass transition temperature from 90 °C to 74 °C, while that of the PAMS beads decreased to 173 °C. It has been reported that the temperature and pressure of the plasma polymerization are about 82 °C and 10 Pa, respectively.[32] The boiling point of FB is 85 °C at atmospheric pressure. With decreasing pressure, the boiling point decreases, and thus the FB can evaporate during plasma polymerization, forming vacuoles. Because the temperature of plasma polymerization is higher than the glass transition temperature of the PS beads, the chain segments of the PS are able to move, which benefits the expansion and agglomeration of the vacuoles to form bigger vacuoles. The glass transition temperature of the PAMS beads is much higher than the plasma polymerization temperature, and so the PAMS chain segments cannot move. Therefore, even if some vacuoles have formed during plasma polymerization owing to FB remaining in the beads, these vacuoles cannot expand. This explains why no large vacuoles were observed in the PAMS-CD multilayer microspheres.

Figure 8 shows the sphericity and surface roughness of the PS-CD and PAMS-CD multilayer microspheres. The cumulative frequency curves of δ_{OOR} for these multilayer microspheres are similar to those of the corresponding beads [compare Figs. 4(a) and 8(a)], which indicates that the coating had no significant effect on sphericity. All the δ_{OOR} values are still less than 1.0 μm, indicating good sphericity. For PS beads, the R_a, R_q, and R_t values increased a little after the coating [compare Figs. 4(c) and 8(b)]. A few bumps appeared on the surfaces of the PS-CD multilayer microspheres [Fig. 8(c)]. For the PAMS beads, both R_a and R_q increased after the coating [compare Figs. 4(c) and 8(b)]. There were many bumps and depressions on the surfaces of the PAMS-CD multilayer microspheres [Fig. 8(c)], probably due to surface defects (vacuoles) on the PAMS beads. Thus, the quality of the surface was reduced after the coating with a CD layer. To improve the surface quality of the CH-CD multilayer polymer microspheres, it is necessary to improve the surface quality of the CH beads and optimize the process of plasma polymerization, which will be the focus of future studies.

© Author(s) 2021

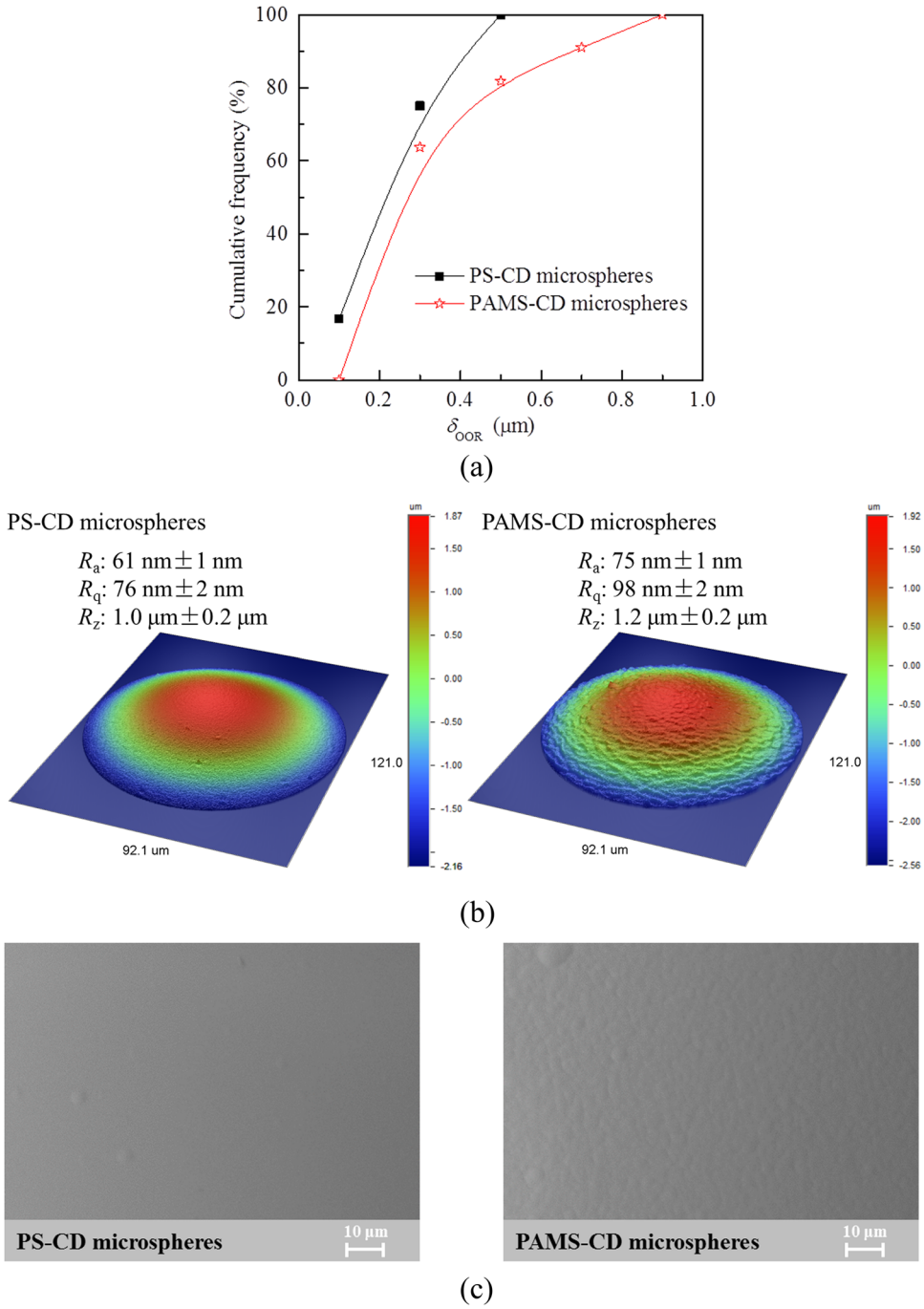

FIG. 8. Effect of PS and PAMS materials on the quality of CH-CD multilayer polymer microspheres: (a) sphericity; (b) surface roughness; (c) SEM micrographs of microsphere surface.

IV. CONCLUSION

Solid CH-CD multilayer polymer microspheres were successfully prepared by a microfluidic technique and plasma polymerization. The diameter variation of the beads and the variation coefficient in each batch were less than 5 μm and 1.0%, respectively, indicating good monodispersity. The diameter of the solid CH beads and the wall thickness of the CD layer were controlled by the size of the corresponding droplets, as well as the CD deposition rate and deposition time, respectively. The effects of the PS and PAMS materials on the

©Author(s) 2021

qualities of both the solid CH beads and the resulting CH-CD multilayer polymer microspheres were investigated. The PS and PAMS beads showed no significant differences in monodispersity and amount of residual solvent, but the PS beads had better sphericity and a smoother surface, probably owing to the differences in molecular structure and molecular weight between the PS and PAMS. Many vacuoles with 5 μm–30 μm diameter appeared in the central region of the PS-CD multilayer microspheres, because the glass transition temperature of the PS beads was lower than the temperature of plasma polymerization and there was some FB remaining in the beads. Therefore, the PAMS beads are more suitable for use as a mandrel for fabricating CH-CD multilayer polymer microspheres. The surface quality was reduced after coating with the CD layer. Further work is therefore necessary to find ways to improve the quality of solid CH-CD multilayer polymer microspheres.

ACKNOWLEDGMENTS

We gratefully acknowledge funding from the National Natural Science Foundation of China (Grant Nos. 51703212 and 52073264), the Open Project of the State Key Laboratory of Environment-Friendly Energy Materials (Grant Nos. 18kfhg03 and 19kfhg02), and a project supported by the CAEP Foundation (Grant No. PY20200117).

REFERENCES

[1]O. A. Hurricane, D. A. Callahan, D. T. Caseyspc *et al.*, "Fuel gain exceeding unity in an inertially confined fusion implosion," Nature **506**, 343–348 (2014).
[2]M. Tabak, J. Hammer, M. E. Glinsky *et al.*, "Ignition and high gain with ultra-powerful lasers," Phys. Plasmas **1**, 1626–1634 (1994).
[3]R. Betti, C. D. Zhou, K. S. Anderson *et al.*, "Shock ignition of thermonuclear fuel with high areal density," Phys. Rev. Lett. **98**, 155001 (2007).
[4]G. Ren, J. Yan, J. Liu *et al.*, "Neutron generation by laser-driven spherically convergent plasma fusion," Phys. Rev. Lett. **118**, 165001 (2017).
[5]D. L. Wilcox and M. Berg, "Microsphere fabrication and applications: An overview," MRS Proc. **372**, 3 (1994).
[6]C. Lattaud, L. Guillot, C.-H. Brachais *et al.*, "Influence of a density mismatch on TMPTMA shells nonconcentricity," J. Appl. Polym. Sci. **124**, 4882–4888 (2012).
[7]A. V. Pastukhov, V. A. Davankov, A. A. Akunets *et al.*, "Hollow poly(alpha-methylstyrene) shells for inertial confinement fusion targets," J. Phys.: Conf. Ser. **907**, 012020 (2017).
[8]D. R. Harding, M. J. Bonino, W. Sweet *et al.*, "Properties of vapor-deposited and solution-processed targets for laser-driven inertial confinement fusion experiments," Matter Radiat. Extremes **3**, 312–321 (2018).
[9]J. Biener, D. D. Ho, C. Wild *et al.*, "Diamond spheres for inertial confinement fusion," Nucl. Fusion **49**, 112001 (2009).
[10]X. T. He, H.-b. Cai, S.-z. Wu *et al.*, "Physical studies of fast ignition in China," Plasma Phys. Controlled Fusion **57**, 064003 (2015).
[11]Y. Mori, Y. Nishimura, K. Ishii *et al.*, "1-Hz Bead-Pellet injection system for fusion reaction engaged by a laser HAMA using ultra-intense counter beams," Fusion Sci. Technol. **75**, 36–48 (2019).
[12]L. Q. Shan, H. B. Cai, W. S. Zhang *et al.*, "Experimental evidence of kinetic effects in indirect-drive inertial confinement fusion hohlraums," Phys. Rev. Lett. **120**, 195001 (2018).
[13]R. Hu, W. T. Kan, X. L. Xiong *et al.*, "Preparation of a deuterated polymer: Simulating to produce a solid tritium radioactive source," J. Nucl. Mater. **492**, 171–177 (2017).
[14]M. Takagi, T. Norimatsu, T. Yamanaka *et al.*, "Development of deuterated polystyrene shells for laser fusion by means of a density-matched emulsion method," J. Vac. Sci. Technol., A **9**, 2145–2148 (1991).
[15]K. Nagai, H. Yang, T. Norimatsu *et al.*, "Fabrication of aerogel capsule, bromine-doped capsule, and modified gold cone in modified target for the fast ignition realization experiment (FIREX) project," Nucl. Fusion **49**, 095028 (2009).
[16]M. F. Liu, Y. W. Huang, S. F. Chen *et al.*, "Progress and challenges in the fabrication of DPS shells for ICF," Matter Radiat. Extremes **4**, 018401 (2019).
[17]M. F. Liu, Y. Q. Zheng, Q. Chen *et al.*, "Controllable production of deuterated polymer beads for ICF," J. Nucl. Mater. **535**, 152159 (2020).
[18]M. F. Liu, S. F. Chen, X. B. Qi *et al.*, "Improvement of wall thickness uniformity of thick-walled polystyrene shells by density matching," Chem. Eng. J. **241**, 466–476 (2014).
[19]M. Takagi, R. Cook, R. Stephens *et al.*, "Decreasing out-of-round in poly(a-methystyrene)mandrels by increasing interfacial tension," Fusion technology **38**, 46–49 (2000).
[20]S. Bhandarkar, R. Paguio, F. Elsner *et al.*, "Understanding the critical parameters of the PAMS mandrel fabrication process," Fusion Sci. Technol. **70**, 127–136 (2016).
[21]F. Zhang, H. B. Cai, W. M. Zhou *et al.*, "Enhanced energy coupling for indirect-drive fast-ignition fusion targets," Nat. Phys. **16**, 810–814 (2020).
[22]H. B. Cai, L. Q. Shan, Z. Q. Yuan *et al.*, "Study of the kinetic effects in indirect-drive inertial confinement fusion hohlraums," High Energy Density Phys. **36**, 100756 (2020).
[23]Y. W. Huang, M. F. Liu, X. N. Wei *et al.*, A method of preparing deuterated polystyrene, China, 2016.
[24]R. C. Cook and A. Nikroo, IR Extinction coefficient measurements of CH and CD GDP shells, USA, 2003.
[25]D. J. Plazek and K. L. Ngai, *Physical Properties of Polymers Handbook*, 2th ed. (Springer, New York, NY, 2007).
[26]L. Lurio, H. Kim, A. Rühm *et al.*, "Surface tension and surface roughness of supported polystyrene films," Macromolecules **36**, 5704–5709 (2003).
[27]L. Ye, M. Liu, Y. Huang *et al.*, "Effects of molecular weight on thermal degradation of poly(α-methyl styrene) in nitrogen," J. Macromol. Sci., Part B. **54**, 1479–1494 (2015).
[28]H. Liu, Z. B. He, J. J. Wei *et al.*, "Chemical structure and mechanical properties of glow discharge polymer films and deuterated glow discharge polymer films," High Power Laser Particle Beams **27**, 032028 (2015).
[29]X. Ai, X.-S. He, J.-L. Huang *et al.*, "The effect of axial ion parameters on the properties of glow discharge polymer in T2B/H2 plasma," J. Phys. D: Appl. Phys. **51**, 095604 (2018).
[30]J. E. G. Lipson and S. T. Milner, "Multiple glass transitions and local composition effects on polymer solvent mixtures," J. Polym. Sci., Part B **44**, 3528–3545 (2006).
[31]H. Jansson, R. Bergman, and J. Swenson, "Role of solvent for the dynamics and the glass transition of proteins," J. Phys. Chem. B **115**, 4099–4109 (2011).
[32]M. Theobald, C. Chicanne, J. Barnouin *et al.*, "Gas etching to obtain germanium doped CHx microshells compatible with the laser megajoule target specifications," Fusion Sci. Technol. **49**, 757–763 (2006).

©Author(s) 2021